



Pulverized coal swirl flames in oxy-fuel conditions: Effects of oxidizer O₂ concentration on flow field and local gas composition

D. Zabrodiec*, J. Hees, G. Möller, O. Hatzfeld, R. Kneer

RWTH Aachen University, Institute of Heat and Mass Transfer, Augustinerbach 6, Aachen 52056, Germany

Received 30 November 2017; accepted 21 June 2018

Available online xxx

Abstract

In an experimental study the effects of varied oxygen concentrations in the oxidizer gas on resulting flow fields, combustion products and general behavior of pulverized coal swirl flames under oxy-fuel conditions have been investigated. Experiments were carried out in a small scale down-fired cylindrical combustion chamber equipped with an annular swirl burner. Studied flames had a constant power output of 40 kW_{th} and O₂/CO₂ oxidizer gas mixtures with O₂ concentrations ranging from 23 to 33 vol%. Detailed two-dimensional flow field measurements are obtained from laser Doppler anemometry (LDA). Velocity profiles (Mean and RMS) have been obtained for all conditions investigated and serve as basis for identification of flow field characteristics. Velocity RMS values are provided as supplementary material. To complement flow field measurements, in-flame gas composition measurements were also conducted using a sampling probe combined with infrared gas absorption analysis via Fourier-transform infrared (FTIR) spectrometry. The results obtained show increased velocities, particularly along the main vortex for flames with increased oxygen contents, while lower velocities are found to occur inside the recirculation regions. The opposite occurs with lower O₂ concentrations, showing significantly reduced velocities in the main vortex, but stronger recirculation than the high oxygen counterparts. This effect is attributed to a modification of the swirl level introduced by the expansion of product gases. Measured NO and CO in-flame concentrations showed significant variations under different O₂ concentrations in the oxidizer.

© 2018 The Combustion Institute. Published by Elsevier Inc. All rights reserved.

Keywords: Oxy-fuel combustion; Pulverized coal; Swirl flame; LDA; FTIR

1. Introduction

In the face of global efforts to reduce its usage, coal remains as one of the cheapest and most

abundant energy sources [1] and most likely will persist as one of the primary energy sources also in the future. Therefore, reduction of atmospheric emissions from coal combustion is currently one of the most important technological challenges. In this scenario, oxy-fuel combustion emerges as one of the plausible technologies to reduce CO₂

* Corresponding author.

E-mail address: zabrodiec@wsa.rwth-aachen.de (D.

Zabrodiec).

<https://doi.org/10.1016/j.proci.2018.06.163>

1540-7489 © 2018 The Combustion Institute. Published by Elsevier Inc. All rights reserved.

emissions by favoring carbon capture and sequestration (CCS) processes [2]. In oxy-fuel combustion, the atmospheric oxidizer (air) is replaced by a mixture of O_2/CO_2 . In case of large combustion systems this is intended to be achieved by recirculating a mixture of flue gas enriched with O_2 . The effect of different O_2/CO_2 concentration mixtures in oxy-fuel pulverized coal (PC) flames has been studied previously by several authors under different experimental configurations. Most of the experimental work on combustion chambers were aimed to find optimal retrofitting conditions. Early conducted works [3,4] proved the feasibility of oxy-fuel combustion. It was also shown that mixtures of O_2/CO_2 , for which temperatures and heat transfer characteristics are similar to those given by the air counterparts, can be easily obtained (with O_2 contents around 23 vol% wet basis). To this day, numerous experimental works have reported values of O_2 vol% in oxidizer mixtures situated between 23 to around 35 vol% (for optimal oxy-fuel retrofit conditions). With 27 vol% being the most recurrent [2].

For reliable velocity measurements in reactive flow fields often laser Doppler anemometry (LDA) is applied, requiring good optical access to the studied flow. Given the construction of coal fired boilers, optical access is usually difficult or even impossible. Nevertheless, flow fields in PC flames have previously been studied by employing LDA. A limited number of authors [5–9] have successfully conducted LDA measurements in PC flames under conventional atmospheric conditions to e.g., characterize the impact of swirl or stoichiometry on the flames. Only recently, LDA measurements have been conducted in PC flames in oxy-fuel conditions, for which most of the work has been dedicated to the validation of numerical simulations [10,11]. More recently, detailed LDA measurements of 60 KW_{th} PC swirl flames under oxy-fuel conditions with O_2 contents of 21 and 25 vol% were conducted and compared against an air reference flame [12]. Probe gas sampling, an intrusive measurement technique that can provide valuable information about the local, in-flame, gas concentration is also employed in the present work to evaluate the influence of O_2 concentrations. Previous works upon PC oxy-fuel flames for gas sampling and concentration measurements can be found in e.g., [13–15], with most of the work dedicated to evaluating flame behavior and measuring concentrations of major products and pollutant species for different O_2 concentrations, different burner configurations and thermal outputs. For a slightly larger burner, recent sampling probe measurements [16,17] revealed the differences between two oxy-fuel cases with respect to a reference air combustion case.

In the present contribution, the combustion behavior of pulverized lignite, when varying oxidizer O_2 concentration over a wider range, is addressed by an experimental study. The selected

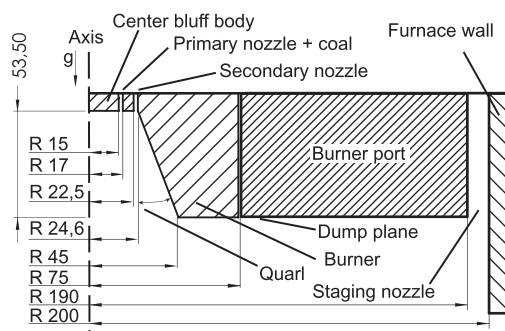


Fig. 1. Half-section of the burner and traversable burner port at the top of the combustion chamber.

experimental configuration can produce flame conditions that resemble those found in practical large coal fired boilers. As swirling flows are difficult to compute given their complexity, measurement data, such as the currently presented, can be of great value to improve the understanding of the complex mechanisms and interactions involved in PC combustion. Therefore, resulting flow fields (by two-component LDA) and in-flame compositions of product gases (by gas sampling) have been measured with high local resolution. Three operating conditions comprising O_2 concentrations of 23, 27 and 33 vol% in the O_2/CO_2 oxidizer mixture are employed.

2. Experimental setup

2.1. Test facility

Experiments were conducted at the combustion test facility of the Institute of Heat and Mass Transfer, RWTH Aachen University. The core of the facility is a down-fired, vertical-cylindrical combustion chamber with an inner diameter of 400 mm and length of 4200 mm [10,18]. The inner walls of the combustion chamber are lined with three layers of ceramic insulation. Electric heating elements embedded in the ceramic allow wall temperatures to be increased and sustained up to 1273 K. The employed swirl burner (see Fig. 1) is mounted at the top-center of the combustion chamber, on a vertically displaceable ceramic burner port. It is composed by two concentric annular nozzles enclosed by a diffuser or quarl [10,11]. Fuel (coal particles) combined with a carrier gas (oxidant mixture with reduced O_2 vol%) is delivered through the primary nozzle, resulting in a non-swirled jet around a central bluff body. Additional oxidant is delivered through the secondary and the staging nozzles. The first is located in the vicinity of the primary, issuing a swirling jet. The staging nozzle is located far from the center-line of the chamber, at the 10 mm gap between the chamber wall and the

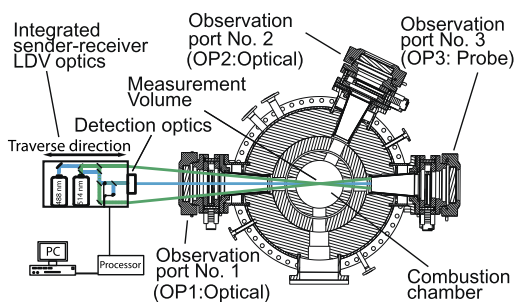


Fig. 2. Chamber cut at the measurement plane (top-view) showing the four observation ports with the LDA system layout.

ceramic burner port. The staging nozzle provides a low speed non-swirled jet, generating staged combustion conditions or extending the operational envelope of the combustion chamber. The burner is water cooled and made of stainless steel. The apex angle of the quartz is $\alpha = 21^\circ$. The hydraulic diameters of primary and secondary nozzles are: $D_{H1} = 4$ mm and $D_{H2} = 4.2$ mm. A set of three radially-arranged observation ports (OP) built at the same transversal plane of the chamber, see Fig. 2, are available for optical and probe measurements. Two ports, OP1 and OP2, are equipped with quartz glass windows allowing optical access to the flame. The third, OP3 is dedicated for probe measurements. All gas flows are controlled by thermal mass flow controllers ($< 1\%$ error). Coal particles are introduced to the primary (carrier gas) with the help of a twin-screw volumetric feeder and a venturi-type ejector. This system can provide a homogeneous and controlled coal particle supply to the burner. Additional information about the experimental setup can be found in [16,19].

2.2. Operating conditions

To address the direct effect of different O_2 concentrations in the O_2/CO_2 oxidizer mixture on flame structure and resulting flow fields, a set of three operating conditions, Oxy23, Oxy27 and Oxy33 with identical nozzle inlet velocities were chosen, with respectively 23, 27 and 33 vol% O_2 concentrations in the oxidizer (Table 1). The coal mass flow supplied to the chamber was kept constant, leading to a constant thermal output of 40 KW_{th} for the three conditions. Two stoichiometric ratios are defined to describe the operation of the combustion chamber: the global stoichiometric ratio (λ_G), is computed by taking into account the total mass of oxygen supplied to the chamber through the three nozzles against the mass of oxygen needed for stoichiometric combustion and the local stoichiometric ratio (λ_L), computed in a similar way as λ_G but taking into account only the oxygen mass supplied through the burner (primary and

secondary nozzles). For all operating conditions the local stoichiometric ratio is kept below one ($\lambda_L < 1$), while $\lambda_G > 1$ is well over-stoichiometric, to assure maximum coal burnout. The O_2 concentration in the primary (carrier gas) is reduced for safety reasons, exact values are given in Table 1. It is important to mention that λ_G values for Oxy27 and Oxy33 are slightly higher than those employed under realistic conditions. For this particular study, λ_L has more significance as measurements are conducted at the fuel-rich near burner regions. Previous studies showed [12] that the staging flow only interacts with the main jet at axial coordinates further down from those studied in the present work. The secondary stream is swirled by angled nozzles inside the burner, providing a geometrical swirl number of $S_g = 0.958$ [20] for all conditions. Rhensish lignite (Germany) was employed for the study. The coal was dried and ground prior to the experiments. Ultimate and proximate analysis composition data are given in Table S2 available within the supplementary material. Laser diffraction particle size analysis revealed a median particle diameter of $D_{50} = 29 \mu\text{m}$, with $D_{10} = 5 \mu\text{m}$ and $D_{90} = 132 \mu\text{m}$.

2.3. Laser Doppler anemometry

LDA measurements were carried out employing a long-range optic system (ILA Laser systems). The system is mounted outside OP1 and is configured as a dual-beam (two-component) arrangement with backscatter detection (Fig. 2). Two diode laser heads (Coherent Genesis CX SLM-Series, 2W each), with wavelengths of 488 nm and 514.5 nm were used. The optical system is capable of delivering 600 mW per beam to the measurement volume. Coal particles, having a polydisperse size distribution, are used as flow tracers. Therefore, the presence of large coal particles in the flow can lead to conditions of important particle-flow slip velocities, which can introduce significant errors in the measurements. To address this issue, the design of the LDA system is optimized to increase laser fluence for small measurement volumes [12]. By doing this, the scattering signals from the larger coal particles can be rejected and detection of signals from smaller particles (better flow tracers) is improved. Doppler-burst signals are collected by the optical lenses of the system and coupled to photomultiplier tubes. Signal sampling and processing is done by an LDA signal processor (Dantec-BSA processor). More detailed information about the LDA system is found in [12]. LDA point measurements were conducted at steps between 1 and 20 mm along the radius of the combustion chamber, delivering radial profiles of axial and tangential velocity components. Radial profiles were measured at five axial distances, $H = 0.3d, 0.5d, 1.0d, 2.0d$ and $4.0d$ from the burner port. Where $d = 49.2$ mm, is the outer diameter of the secondary nozzle.

Table 1
Operating conditions.

Parameter	Oxy23	Oxy27	Oxy33
Coal mass flow rate [kg/h]	6.7	6.7	6.7
Volume flow rate of primary stream ^a [m ³ /h]	9.4	9.4	9.4
O ₂ fraction of primary stream [vol.-%]	20.7	24.4	29.8
Temperature of primary stream [°C]	25	25	25
Volume flow rate of secondary stream ^a [m ³ /h]	8.8	8.8	8.8
Volume flow rate of staging stream ^a [m ³ /h]	23.1	23.1	23.1
O ₂ /CO ₂ secondary and staging streams [vol.-%]/[vol.-%]	23/77	27/73	33/67
Swirl no. secondary stream ^b	0.958	0.958	0.958
Temperature of secondary / staging stream [°C] / [°C]	40/900	40/900	40/900
Local / global stoichiometric ratio ^a (λ_L/λ_G)	0.51/1.19	0.6/1.4	0.73/1.71
Bulk velocity primary stream ^a (U_I) [m/s]	12.99	12.99	12.99
Bulk velocity secondary stream ^a (U_{II}) [m/s]	7.87	7.87	7.87
Bulk velocity staging stream ^c (U_{ST}) [m/s]	2.25	2.25	2.25
Momentum flux primary stream ^{a,d} [kg.m/s ²] · 10 ⁻³	87.4	86.7	85.7
Momentum flux secondary stream ^{a,d} [kg.m/s ²] · 10 ⁻³	36.1	35.8	35.2
Momentum flux staging stream ^{a,d} [kg.m/s ²] · 10 ⁻³	6.3	6.2	6.2

^a STP = Standard temperature (0 °C) and pressure (1.013 bar).

^b Geometrical swirl numbers, estimated from the geometry of the burner.

^c Calculated for a temperature of 900 °C and a pressure of 1.013 bar.

^d Initial momentum of the incoming gases at the exit section of the nozzles.

Between 10⁴ and 10⁵ particle counts were taken at each point in order to guarantee over 99% statistical confidence.

Acquisition time-series of 45–60 s were employed to average out the weight of random systematic fluctuations. A theoretical particle slip error estimation was previously conducted in [12] taking into account similar coal particle size distribution and flow velocities. The estimation of the slip-associated error is 2%. The systematic measurement error of the LDA system was assessed with a dynamic calibration target (Optolution - ILA, LDV turn-table velocity standard). The calibration target when placed at the center of the LDA measurement volume showed an error of 0.5% for both velocity components. Further on, aberrations in the fringe pattern of the measurement volume showed an error of 5% at both ends of the measurement volume. Therefore, a conservative estimation of the LDA measurement error is in the order of 7% of the measured velocity. Although the flows are assumed to be axisymmetrical, measurements revealed slight asymmetries, which amount to maximum 10% of values measured at symmetrically opposite points.

2.4. Gas sampling probe system

An oil-tempered gas sampling probe [17] was employed in order to estimate the product gas composition at different locations in the studied flames. The probe has an outer diameter of 33 mm, an inner diameter of 6 mm and a total length of 2600 mm. The probe was mounted at OP3 (see Fig. 2) and radially driven into the combustion chamber by a traverse system. Product gases were

sampled through the tip of the probe at a continuous volume flow of 50 l/h using a heated vacuum pump. The sampled gas was transported through electrically heated (PTFE) flexible hoses, first going through a fine particle filter before entering the sample gas cell of a Fourier transform infrared (FTIR) spectrometer (Gasetm DX-2000). All active components in the sampling lines including the sampling probe were heated to 473 K to prevent water condensation and to minimize condensation of higher ranked hydrocarbons (e.g., tar compounds). The concentration of major product species was estimated by evaluating their respective absorption bands in the infra-red spectra provided by the FTIR spectrometer [21]. Evaluated gas concentrations included two product species: carbon monoxide CO, and nitric oxide NO.

Radial concentration profiles were composed of point measurements taken along the radius of the chamber with steps of 25 mm between 0 (center) and 200 mm (wall). Point acquisition was done using random radial positions to reduce systematic errors. At each measurement position, gas was sampled and evaluated for at least 5 min, with 2 min buffer time before and after measurement to guarantee that sampled gas from a previous position is purged out of the system. For each data point, absorption spectra were acquired by the FTIR at a rate of 1 Hz and internally averaged in the instrument for 20 s measurement time. Measurements were conducted at three axial planes relative to the burner, H = 0.5d, 1.0d and 2.0d matching three of the axial locations of the LDA measurement.

The calibration of the FTIR is done by employing different known concentrations of single gases at a temperature of 453 K and an absolute

pressure of 100 kPa. Resulting errors in the evaluation of binary mixtures (test gas in N_2) have been estimated to be less than 7.5% [22]. Precision of determined concentrations is further reduced in multi-component gas mixtures e.g., due to overlapping absorption bands or line broadening effects. To compensate for this, wave number regions for each single gas species have been analyzed and optimized for measurements of oxy-fuel flue gas mixtures. Real precision depends on the actual wave number range employed as well as the evaluated gas concentration. Therefore no exact value can be specified.

To estimate the error from probe intrusive effects in the flow, combined LDA measurements with the probe at different radial positions in the chamber were conducted. By placing the probe at different radial positions and measuring flow field differences near the probe tip, errors in the flow field were found to be within 10% in mean velocity when protruding with the probe less than half-diameter of the combustion chamber. When placing the probe beyond the center of the combustion chamber, differences in the flow field larger than 40% were observed. This is valid for all measurements conducted at $H = 1.0d$ and further downstream from the burner. Therefore, in order to avoid significant intrusion of the flow, probe measurements were limited only to the first half-diameter of the combustion chamber.

3. Results and analysis

3.1. Flow field measurements

Measurement results from Oxy27 (reference condition) are shown in Fig. 3. The profiles provide an archetype for all three studied flames, given that common features from annular swirling flows, such as the main vortex (MV), internal and external recirculation zones (IRZ and ERZ), and the internal and external shear layers (ISL and ESL) are clearly identified and are similar for the three conditions. Also, the non-swirled staging flow (SF) near the chamber walls is observed.

The axial velocity profiles (Fig. 3a), show that the location of the MV gradually shifts towards the center of the chamber indicating a contraction of the flame. Flame contraction is accompanied by a gradual relaxation of the axial mean velocity profile, where peaks decrease and broaden. Tangential mean velocities (Fig. 3b) show a slightly different pattern. As the MV shifts towards the center and the flame contracts, peak tangential velocities increase until reaching a maximum at $H = 1.0d$ and then gradually decrease similar to the axial velocity. The IRZ (see Fig. 3a) is extended between $H = 0.3d$ and $1.0d$, but collapses at an undetermined position between $H = 1.0d$ and $2.0d$.

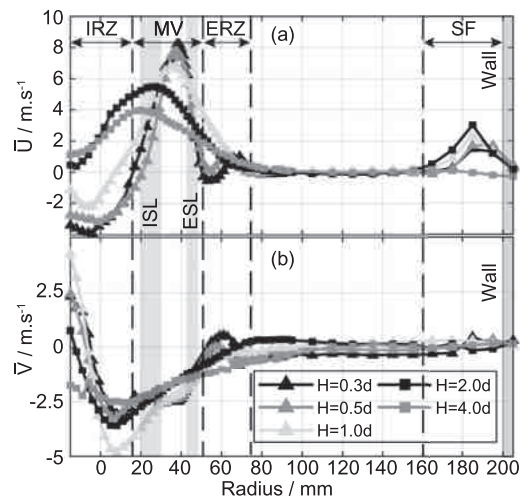


Fig. 3. Measured mean axial (\bar{U}) and mean tangential (\bar{V}) velocity components for Oxy27 condition at 5 heights ($d = 49.2$ mm), indicated regions are based on the $H = 0.3d$ profiles.

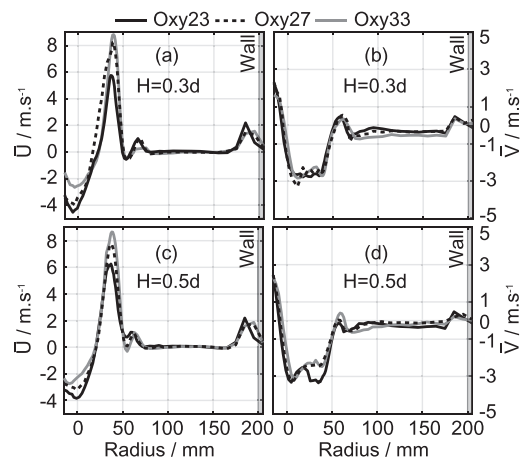


Fig. 4. Mean velocity axial and tangential velocity components at $H = 0.3d$ (a,b) and $H = 0.5d$ (c,d) from the burner port. Symbols have been omitted for improved interpretation.

A small ERZ is also observed between $R \approx 50$ and 60 mm in the $H = 0.3d$ and $0.5d$ profiles.

To evaluate the effect of different O_2 concentrations, Figs. 4 and 5 present a comparison of mean velocity profiles at $H = 0.3d$ and $H = 0.5d$ (near-burner regions), and $H = 1.0d$ and $H = 2.0d$ (mid-range from the burner) for all studied conditions. In all cases, higher axial velocities in the MV were observed with increased O_2 concentrations. Peak axial velocities measured at the MV show that Oxy33 produced higher overall velocities at the MV across all measured axial positions. Oxy27 follows with intermediate values and the lowest overall velocities at the MV were measured

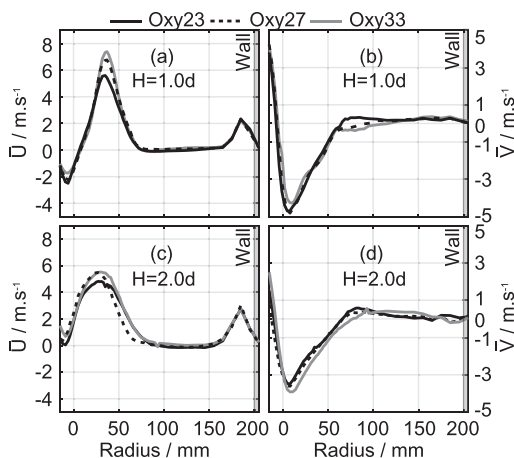


Fig. 5. Mean velocity axial (a,c) and tangential (b,d) velocity components at $H = 1.0d$ and $H = 2.0d$ from the burner port. Symbols have been omitted for improved interpretation.

for Oxy23. The maximum values of Oxy33 ($\bar{U} = 8.82 \text{ m/s}$) and Oxy27 ($\bar{U} = 8.22 \text{ m/s}$), both were measured at $H = 0.3d$. The maximum axial velocity for Oxy23 ($\bar{U} = 6.24 \text{ m/s}$) was found in the MV at $H = 0.5d$. Peak values in the IRZ show the opposite trend to the one in the MV, with higher recirculation velocities near the center for decreased O_2 concentrations. Mean tangential velocities near the burner (Fig. 4b, d) show the presence of two peaks ($R = 11$ and 38 mm), which merge further downstream as the rotation of the flow increases (at $H = 1.0d$, Fig. 5b). The measured maximum tangential velocities were all found at $H = 1.0d$. Velocity RMS values from all measured profiles can be found in Figs. S1 and S2, provided as supplementary material. In addition, particle temperatures, measured by employing an optical probe, are also given in Figure S3. A detailed description of the particle temperature measurement method can be found elsewhere [19].

The Oxy23 condition also showed a unique feature, an increase of axial velocity at the MV from $H = 0.3d$ to $0.5d$, which is attributed to further gas expansion and acceleration occurring between these two axial locations. This behavior was only observed in Oxy23, maximum velocities measured for Oxy27 and Oxy33 generally revealed a decaying trend after $H = 0.3d$. Measured particle temperatures at $R = 0 \text{ mm}$ and $H = 1.0d$ (Fig. S3) gradually increase from 1164 K in Oxy23 to 1562 K in Oxy33. Measured RMS values show no consistent trend with O_2 variations. Nevertheless Oxy23 and Oxy27 showed two intense narrow RMS peaks (Fig. S1b and S1d) at $R = 75 \text{ mm}$ between $H = 0.3d$ and $0.5d$. These peaks are located directly at the ERZ of the flame and are possibly attributed to flow intermittency.

Overall LDA measurement results reveal that the general characteristics of the studied flows are similar. Nevertheless, significant differences in the flow fields have been identified. In particular, the differences in mean velocity observed in the IRZ and MV. First, it is fundamental to acknowledge that all studied flames have the same initial bulk velocities U_I and U_{II} (cf. Table 1) and initial swirl level. Also a slight reduction in the momentum of the gases and increment in the viscosity is expected with increasing O_2 content. Therefore, the higher axial velocities experienced by i.e., Oxy33 is attributed to the more intense initial expansion of the gases, product of the combustion reactions, to later have reduced velocities at the IRZ due to a reduction of the actual swirl level experienced by the flow and the slightly higher relative viscosity of the gas mixture. In a similar way, reduced O_2 (i.e., Oxy23) concentrations lead to comparatively less intense initial gas expansion which keeps the actual swirl level of the flow higher at lower viscosity of the mixture, thus enhancing the intensity of the IRZ.

3.2. Gas composition measurements

In order to complement data from flow field measurements, in-flame gas composition measurements were conducted (Section 2.4). Figure 6 shows radial profiles of CO and NO measured at three different axial planes $H = 0.5d$, $1.0d$ and $2.0d$. From the radial profiles of CO and NO (Fig. 6) two regions can be identified: (i) the main reaction zone (flame), from $R = 0$ to $\approx 80 \text{ mm}$ and (ii) the outer dilution zone, beginning at $R \approx 80 \text{ mm}$ extending to the chamber walls at $R = 200 \text{ mm}$.

CO is an intermediate combustion product in PC flames [23,24], and its production is largely subjected to the local availability of O_2 molecules and the oxidation of solid carbon at the particles. CO measurements profiles show that local concentrations are increased with lower O_2/CO_2 mixtures, also hardly any CO or very low levels are measured outside region (i), most of it is confined within the flame. This is due to the fact that most of CO is being produced and consumed at regions with high coal particle concentrations (fuel-rich) and most of the coal particles are confined within the swirling jet. Compared to Oxy23 and Oxy27, Oxy33 measurements show a significant drop in overall CO concentrations, to the point that at $H = 2.0d$ almost no CO is left.

Locally measured NO originates from nitrogen included in the coal and is released during the different stages of combustion. With a present nitrogen content of 0.91 w\% in the coal (See Table S1), measured profiles (Fig. 6) show a significant increment of NO with almost double the values measured in Oxy33 than Oxy23. This can be directly attributed to the higher temperatures produced with higher O_2 concentrations [13] and the higher avail-

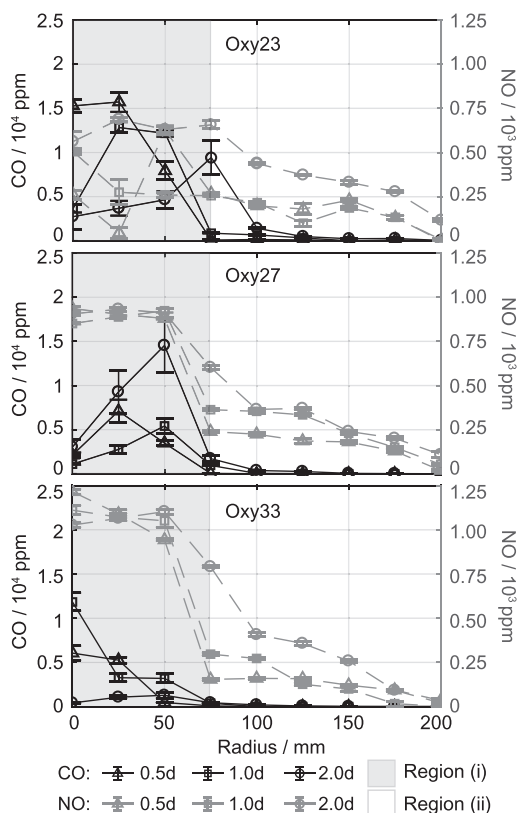


Fig. 6. Radial gas concentration profiles of CO and NO. For Oxy23, Oxy27 and Oxy33 conditions, error bars show the standard deviation.

ability of O_2 molecules. Profiles from Fig. 6 show that contrary to what was observed on the CO profiles, NO is not confined to region (i) but also diffuses significantly across region (ii). In all three studied conditions, measured NO values gradually increase from $H = 0.5d$, reaching their maximum concentrations at $H = 2.0d$.

The transition between zones (i) and (ii) in Fig. 6 (located between $R \approx 60$ and 100 mm) is coincident with the end of the ERZ at $H = 0.5d$ (Fig. 4) and the end of the ESL in $H = 1.0d$ and $H = 2.0d$ (Fig. 5).

4. Conclusions

Measurements (LDA and Gas Sampling Probe) were conducted for a set of three 40 KW_{th} swirl PC flames under oxy-fuel conditions (see Table 1). Although the general structure of the three flames was similar, higher velocities were measured with increased O_2 content in the main vortex (MV), but with smaller velocities in the IRZ compared to lower O_2 conditions. Further on, lower O_2 concentrations increase recirculation velocities in the

IRZ (almost 50% higher for Oxy23 than for Oxy33) while lower axial velocities were measured at the MV. This could be attributed to the more intense expansion of the product gases under high O_2 conditions. This increases the axial momentum (axial velocity) of the product gases, resulting in a reduction of the actual swirl levels in the flame. Thus, the local modification in the swirl combined with small variations in mixture viscosity can be accounted for the observed differences. A general comparison of the measured flow fields show that the overall structure of the flows are mostly determined by the inlet conditions. The structural variations introduced by the combustion reactions for the studied cases are less significant than features generated by the flow fields. If flames are to be studied under varied O_2/CO_2 mixtures but identical stoichiometric ratios, special care has to be taken to inlet conditions and consequent aerodynamic differences in the flow.

Higher yields of NO were measured under increased O_2 , possibly due to the higher availability of O_2 molecules and higher flame temperatures. Local CO concentrations increased under lower O_2 conditions. The Oxy23 condition, with the lowest O_2 content, showed significant evidence of staged combustion: Higher CO values and further acceleration were measured at locations where the other cases were found to decelerate.

Results from the present contribution provide a valuable insight into the effects of O_2 content in oxy-fuel flames. Furthermore, LDA and gas composition data, with adequate resolution, for three different test cases (under well documented operating conditions) are provided, including velocity RMS profiles and particles temperatures as supplementary material.

Acknowledgments

This work has been financed by the German Research Foundation (DFG) within the framework of the SFB/TRR 129 “Oxyflame”. The authors further acknowledge the help of colleagues from RWTH Aachen University: S. Pielsticker, A. Massmeyer, M. Ecker, T. Grooten, B. Thalheim, T. Kretitzberg, B. Gövert, M. Höfler for providing valuable contributions to the experimental data gathering process. The re-design of the burner by L. Becker (RSM, TUD) also is gratefully acknowledged.

Supplementary material

Supplementary material associated with this article can be found, in the online version, at doi:10.1016/j.proci.2018.06.163.

References

- [1] IEA, *Coal Information 2016*, International Energy Agency (IEA), 2016.
- [2] L. Chen, S.Z. Yong, A.F. Ghoniem, *Prog. Energy Combust. Sci.* 38 (2) (2012) 156–214.
- [3] R. Payne, S. Chen, A. Wolsky, W. Richter, *Combust. Sci. Technol.* 67 (1989) 1–16.
- [4] A.M. Wolsky, E.J. Daniels, B.J. Jody, *J. Air Waste Manag. Assoc.* 41 (4) (1991) 449–454.
- [5] G. Pröbstle, W. Wenz, *Combust. Flame* 72 (2) (1988) 193–203.
- [6] P. Ereaut, M. Gover, *J. Inst. Energy* 64 (1991) 135–142.
- [7] R. Weber, J. Dugué, A. Sayre, B. Visser, *Symp. (Int.) Combust.* 24 (1) (1992) 1373–1380.
- [8] P. Jensen, P. Ereaut, S. Clausen, O. Rathmann, *J. Inst. Energy* 67 (1994) 37–46.
- [9] L.M. Pickett, R.E. Jackson, D.R. Tree, *Combust. Sci. Technol.* 143 (1999) 79–107.
- [10] D. Toporov, P. Bocian, P. Heil, et al., *Combust. Flame* 155 (2008) 605–618.
- [11] P. Heil, D. Toporov, H. Stadler, S. Tschunko, M. Förster, R. Kneer, *Fuel* 88 (7) (2009) 1269–1274.
- [12] D. Zabrodiec, L. Becker, J. Hees, et al., *Combust. Sci. Technol.* 189 (10) (2017) 1751–1775.
- [13] E. Croiset, K. Thambimuthu, A. Palmer, *Can. J. Chem. Eng.* 78/2 (2000) 402–407.
- [14] H. Liu, R. Zailani, B. Gibbs, *Fuel* 84 (2005) 833–840.
- [15] J.-P. Bohn, M. Blume, A. Goanta, H. Spliethoff, *Fuel* 90 (10) (2011) 3109–3117.
- [16] J. Hees, D. Zabrodiec, A. Massmeyer, M. Habermehl, R. Kneer, *Flow Turbul. Combust.* 96 (2) (2016a) 417–431.
- [17] J. Hees, D. Zabrodiec, A. Massmeyer, et al., *Combust. Flame* 172 (2016b) 289–301.
- [18] H. Stadler, D. Christ, M. Habermehl, et al., *Fuel* 90 (2011) 1604–1611.
- [19] D. Zabrodiec, J. Hees, A. Massmeyer, et al., *Fuel* 201 (2017) 136–147.
- [20] A. Gupta, D. Lilley, N. Syred, *Swirl Flows*, Energy and engineering science series, Abacus Press, 1984.
- [21] D. Martin, P. Medvecz, K. Nichols, *Appl. Spectrosc.* 47 (1993) 1898–1906.
- [22] S. Pielsticker, B. Goevert, T. Kreitzberg, M. Habermehl, O. Hatzfeld, R. Kneer, *Fuel* 190 (2017) 420–434.
- [23] L.D. Smoot, D.T. Pratt (Eds.), *Pulverized-Coal Combustion and Gasification*, Plenum Press, pp. 149–167.
- [24] L.D. Smoot, D.T. Pratt (Eds.), *Pulverized-Coal Combustion and Gasification*, Plenum Press, pp. 133–147.